The Breakup of Langmuir Circulation and the Instability of an Array of Vortices

S. A. THORPE

Department of Oceanography, The University, Southampton, United Kingdom

(Manuscript received 1 February 1991, in final form 20 June 1991)

ABSTRACT

The presence and pattern of Langmuir circulation can be detected using side-scan sonar. The circulation creates bands of subsurface bubbles, scatterers of high-frequency sound, in the downwelling region beneath the surface convergence. The bands are clearly visible in sonographs. A common process of development is for them to join in pairs.

The stability of the circulation pattern is examined, making a number of simplifying assumptions. In particular, we represent the Langmuir cells as linear vortices. These are subjected to small disturbances. When these are restricted to two-dimensional motions normal to the axes of the vortices, stable modes are found in part of the parameter range in which the windrow separation is large in comparison to an appropriate depth scale, such as the depth of the vortex core in a very deep mixed layer or the depth of the thermocline or lake when this is finite. These modes are destabilized to collective instabilities when three-dimensional motions are permitted. The dominant mode of instability in the parameter range in which Langmuir circulation is mostly found is, however, a pairing mode (consistent with the sonar observations), having an axial wavelength similar to the observed downwind extent of windrows.

The growth rates of the instability agree favorably with those expected from observations. Further study is appropriate in view of the possible importance of this instability as a mechanism for dispersion of floating material or diffusion of soluble matter in the sea.

1. Introduction

The role of Langmuir circulation in promoting vertical transport and diffusion in the upper-ocean boundary layer has been described at length (Langmuir 1938; see also reviews by Pollard 1977 and Leibovich 1983), although its effects are still poorly understood or quantified. Its possible importance in horizontal dispersion has, however, been recognized only relatively recently (Csanady 1974; Faller and Auer 1987).

Langmuir circulation consists of a quasi-steady pattern of parallel vortices, usually oriented downwind, and of alternating sense of circulation or vorticity. Flotsam accumulates on the surface of the water in the convergent motion between alternate vortex cells, where "windrows" are formed above downward-moving water at the cell boundaries. This floating material will remain in the intercell position and separated from that in adjacent windrows, but being carried downwind, until it is cast upon the leeward shore or, as we shall suppose here, until the local circulation pattern breaks up. Similarly, a passive, neutrally buoyant tracer may tend to be contained within one circulation cell and so constrained in its dispersal zone; it will be passed only slowly to neighboring cells by intercell turbulence on scales smaller than the cell dimensions, at least until the circulation pattern breaks down, when a relatively rapid lateral dispersion to adjoining cells may occur. Dispersion across the wind direction of floating material, passive tracers, or even dissolving and rising bubbles or swimming organisms may thus depend critically on the breakdown of the circulation pattern, how often this occurs, and on the transfers that then take place between neighboring cells. This mechanical concept of medium-scale lateral dispersion (medium between the subcell-scale and mesoscale eddy turbulence of a scale much larger than the cell dimensions) offers the possibility of improving the parameterization of subgrid-scale effects in models of turbulent diffusion in the ocean mixing layer and of extending their predictive application to tracers of different kinds.

How then do the circulation cells break up or amalgamate? Advances in the application of sonar to the study of the upper ocean (Thorpe and Hall 1983; Thorpe et al. 1985) have the potential to address this question. Figure 1, kindly provided by M. Curé, illustrates the information now available. This is a sonograph obtained using side-scan sonar mounted on a fixed tripod on the steeply sloping side of freshwater Loch Ness at a depth of 40 m. The mean depth is 150 m. The 90-kHz sonar produces a beam that is tilted up at 20° from the vertical. The beam is some 2 deg wide in the horizontal and 46 deg in the vertical plane. It points across the 1-km-wide loch and is approxi-

Corresponding author address: Prof. Steve A. Thorpe, The University, Department of Oceanography, Southampton, S09 5NH, United Kingdom.

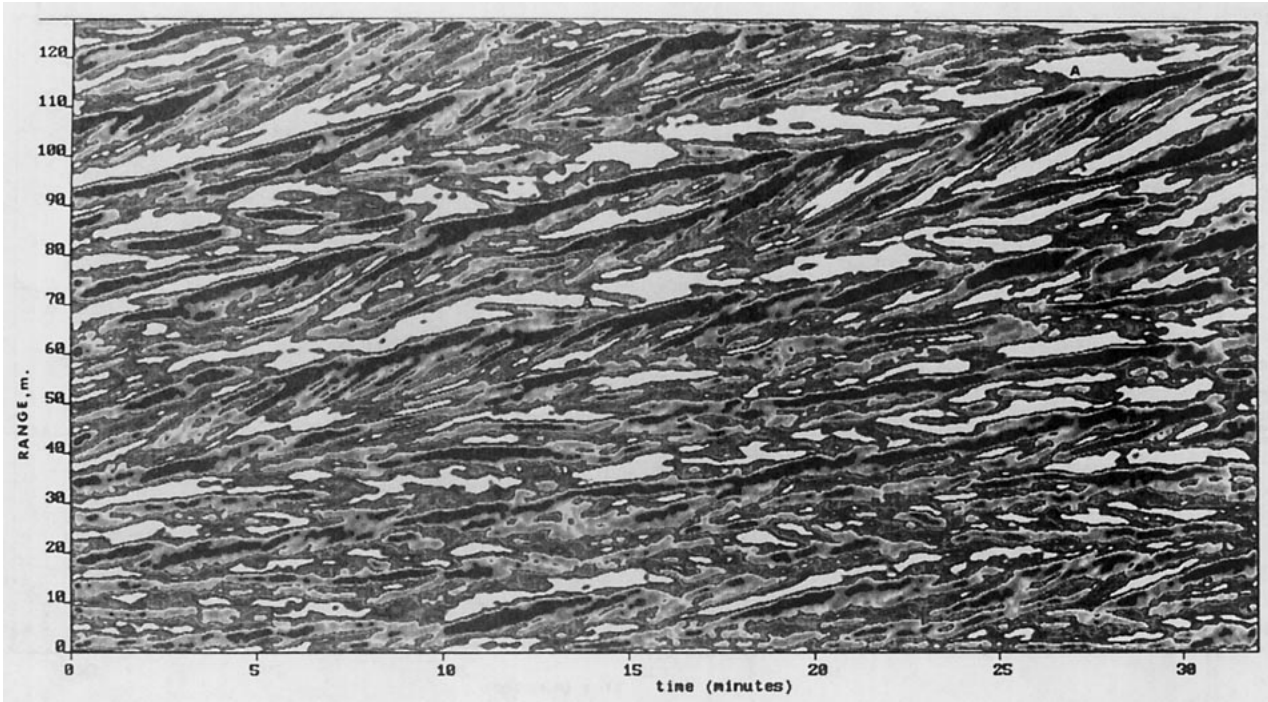

FIG. 1. Sonograph showing range of acoustic targets versus time made from a sonar pointing across the wind direction in wind speeds of 13 m s^{-1}. The bands are due to linear clouds of bubbles in the surface convergence zones and neighboring descending current regions of Langmuir circulation cells. Convergent patterns are seen, for example at A. These patterns may be seen more clearly by viewing the figure from the left at a low angle.

mately normal to the loch axis. The sonograph was made in a wind speed of about 13 m s^{-1} and fetch of some 20 km. It is a range-versus-time display, and shows bands due to sound reflected from clouds of subsurface bubbles caused by breaking waves and carried into zones below the windrows (themselves often composed of floating bubbles) by the locally convergent pattern of flow set up by the Langmuir circulation. There they form acoustic targets with large scattering cross sections to high-frequency sound, which are visible on the sonograph (Thorpe 1984).

Two scales of structure can be seen in the bands. At *A*, for example, bands with a relatively small separation (typically 2–6 m) have an apparent motion toward a larger-scale, more persistent neighboring band. They amalgamate with the larger band in about 2–3 min. Some of these small bands are bubble clouds left by waves breaking in, or close to, the sonar beam that do not have extensive downwind extent. Their cross-wind advection does, however, provide a measure of convergence speed in the larger-scale structure, typically 5 cm s^{-1}. Multiple scales of windrows have frequently been observed before, for example, at sea (Weller and Price 1988) and in the laboratory (Faller and Caponi 1978), and they are found in numerical models (Leibovich and Paulucci 1980). The smaller scales appear to be advected by the larger scales.

The bands with larger separation seen in the sonograph are typically 15–20 m apart and persist for 15–30 min. They are usually associated with floating foam, which is visible in windrows on the surface. They are observed to have a downwind extent of order 10 times their separation scale. Curé has used an objective program to identify the mean pattern of the larger bands visible in Fig. 1, and this is shown in Fig. 2. Several particular features are evident. The bands appear to amalgamate or join in pairs (e.g., at places marked by arrows), but not to bifurcate. Some bands appear to terminate with no amalgamation, and this occurs about as often as does pairing. There is also a generally observed drift of the bands in a direction to the right of wind direction—a tendency observed and remarked on earlier (Thorpe and Hall 1982) in relation to windrows. This may be a Coriolis effect. It seems unlikely to be due to waves or instability, which would be expected to force motion equally in either direction. It is, however, with the termination and amalgamation of the larger-scale bands that we are concerned here.

In the theoretical discussion that follows, we imagine that the pattern of flow found in Langmuir circulations has already been established in a quasi-steady state and can be represented by a linear array of parallel, equally spaced vortices of alternating signs lying on a plane parallel to the water surface and representing the large-scale patterns observed in the sonograph. Our objective is to provide a basis for understanding the possible modes of breakdown of the circulation pattern, and hence, how and on what time and space scales lateral diffusion may occur, by examining the stability of the vortex array. We shall suppose that the mechanism

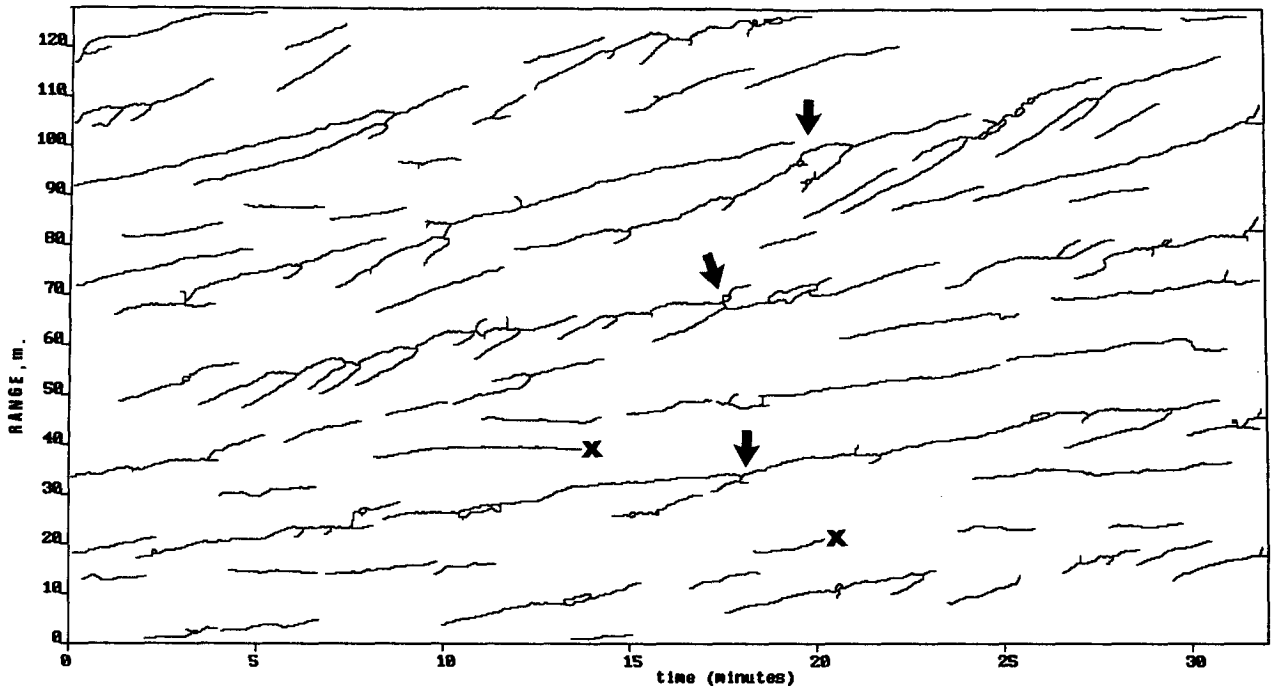

FIG. 2. The banded pattern seen in Fig. 1 showing the amalgamation or pairing of bands. This was obtained by identifying and connecting regions of maximum backscatter. Arrows mark places where major bands amalgamate, and crosses where they terminate.

that generated the vortices is no longer operative, or rather that forcing is no longer coherent or is diminished to such an extent that the established vortices are free to interact. The precise generation mechanics of Langmuir circulation (reviewed by Leibovich 1983) are still poorly understood. The *assumption* that forcing is no longer dominant at the time of observation of the instability of the cells may in general be unjustified, but it offers simplification as a first step toward a more exact description in which some balance between forcing and instability will have to be considered. We shall conclude that two classes of instability appear most likely: the first is a pairing mechanism similar to that observed in the instability of a vortex sheet or free shear layer, and the second a collective mode in which many vortices may be involved. We estimate the magnitude of the growth rates of instability and discuss the predictions in the light of observations.

The approach here is distinct and quite different from that of Leibovich and collaborators (Moroz and Leibovich 1985; Leibovich et al. 1989), who have examined the nonlinear stability of flows in which cells develop, using a truncated set of equations and confining attention to two-dimensional disturbances. A variety of possible states has been described in that analysis, including period-doubling bifurcations and period-doubling cascades to chaotic motion. Some conditions found in constrained flows are not reproduced when lateral boundary conditions are relaxed, and traveling waves and other novel steady states become evident. (The traveling waves are of particular interest in view of the commonly apparent cross-wind migration of windrows.) Features of the analysis absent in this study are the maintenance of constant and continual forcing by stress or by thermal boundary conditions and finite (eddy) viscosity. Here we neglect the effects of forcing and of the turbulent diffusion of momentum, but include those three-dimensional effects that, in view of the foreseen application to lateral dispersion, are essential.

2. The models

a. *An array of vortices near a boundary in water of infinite depth*

Consider an array of line vortices each parallel to the y axis and of alternating sign. The vortices are located at $x = nl$; $n = 0, \pm 1, \pm 2, \cdots$ and lie in a horizontal plane, $z = -h$, so that each is distance l from its neighbor and all are at a distance h from a rigid, free-slip boundary located at $z = 0$. We represent the free surface of the ocean or lake by this rigid plane and ignore vertical displacements, recognizing that in practice those generated by the motions associated with Langmuir circulation, although sometimes in excess of 20 cm s^{-1} (Weller and Price 1988), are small. The fluid is supposedly inviscid and homogeneous with no density variation. The flow field may be represented by an unbounded fluid in which a second array of "image" vortices of signs opposite to the first is located at

$x = nl$, $z = h$ (Fig. 3). The velocity at the position of the rigid boundary, $z = 0$, is then everywhere in the horizontal plane, so satisfying the boundary condition of zero vertical flow. The vortices are supposed to be perturbed by a wave in the x-direction (a two-dimensional disturbance) or by a disturbance with components in both x and y. We may represent any general disturbance by Fourier superposition, and it is therefore necessary to consider only disturbances that are periodic in x and y.

Lamb (1932) provides a thorough description of a procedure to establish the stability in the case of two-dimensional disturbances to an array of vortices all of the same size, referring to earlier work, particularly that of von Kármán (1911, 1912). The extension of the procedure to include three-dimensional perturbations, developed by Rosenhead (1930) and Crow (1970), is carefully described by Robinson and Saffman (1982, hereafter referred to as RS), who present an extensive review of the literature, much of which was directed toward an understanding of the stability of the Kármán vortex street. We shall here closely follow the notation and method adopted by RS, to which the reader is referred for details, and for brevity offer only an outline of the procedure. The geometry considered is similar to the symmetric double row of vortices examined by RS, the main difference being that here the signs of the vortices alternate. Because of its symmetry, the undisturbed state is one in which the vortices are at rest; the net motion induced at the position of any vortex is zero.

Consider first a two-dimensional perturbation, as described by Lamb, in which the vortices are moved to positions $(nl + x_n, -h + z_n)$ in the (x, z) plane. To satisfy the boundary condition the image vortices move to positions $(nl + x_n, h - z_n)$. The velocity induced at position (x, z) by a vortex of strength Γ located at the origin is

$$\left(\frac{\Gamma y}{2\pi(x^2 + y^2)}, \frac{-\Gamma x}{2\pi(x^2 + y^2)}\right).$$

The motion of an individual vortex is then found by summing the contributions of all other vortices, including the image vortices, to determine the motion at its location. Linearization is then carried out supposing that the displacements (x_n, z_n) are small, to derive an expression relating the rate of change with time of the position of a selected vortex, say, that originally at $(0, -h)$, which subsequently has coordinates x_0 and z_0 as a linear function of the displacements of all vortices.

We now put

$$x_n = \alpha e^{in\phi} \quad \text{and} \quad z_n = \beta e^{in\phi}, \tag{1}$$

where $0 < \phi < 2\pi$ is related to the wavenumber of the disturbance along the line of vortices, ϕ/l, or to the wavelength, $2\pi l/\phi$. The equations then take the form

$$\frac{2\pi l^2}{\Gamma}\frac{d\alpha}{dt} = -B\alpha + (C - A)\beta \tag{2}$$

and

$$\frac{2\pi l^2}{\Gamma}\frac{d\beta}{dt} = -(A + C)\alpha - B\beta, \tag{3}$$

where

$$A = \frac{\pi^2}{4}\left[\frac{1}{\cosh^2 k\pi} + \frac{1}{\sinh^2 k\pi}\right] - \frac{\phi^2}{2},$$

$$B = \frac{i}{4}\left[\frac{2\pi\phi\,\cosh k(\pi - 2\phi)}{\sinh k\pi} - \pi^2\frac{\sinh 2k\phi}{\sinh^2 k\pi} - \frac{\pi\phi\,\sinh k(\pi - 2\phi)}{2\cosh k\pi} - \frac{\pi^2\sinh 2k\phi}{4\cosh^2 k\pi}\right],$$

$$C = \frac{\pi\phi\,\cosh k(\pi - 2\phi)}{2\cosh k\pi} - \frac{\pi^2\cosh 2k\phi}{4} \times\left(\frac{1}{\cosh^2 k\pi} + \frac{1}{\sinh^2 k\pi}\right) - \frac{\pi\phi\,\sinh k(\pi - 2\phi)}{2\sinh k\pi},$$

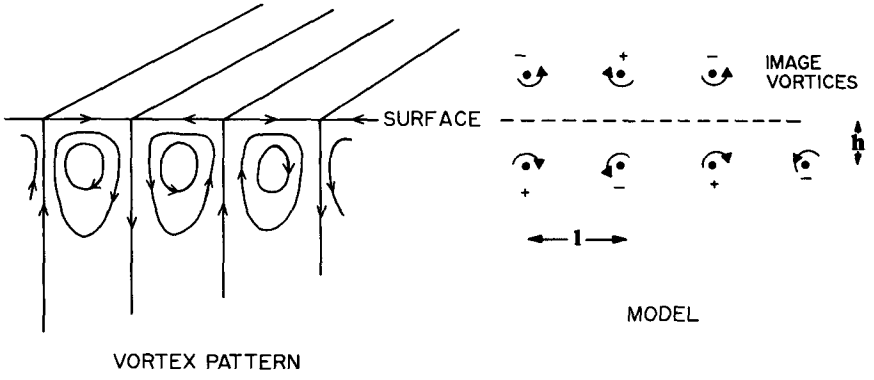

FIG. 3. Sketch of the vortex pattern and model image field for a set of parallel vortices at a distance h from a plane boundary.

and $k = h/l$. [The coefficients may be derived from formulas given by Lamb (1932), recognizing that the configuration of vortices is a combination of two symmetric arrays of corotating vortices with spacing $2l$, the sets being offset by l, or derived using summation formulas given by Bromwich (1955).]

Seeking solutions proportioned to $\exp(pt)$ we find $p = (\Gamma/2\pi l^2)[-B \pm (A^2 - C^2)^{1/2}]$, so, noting that B is pure imaginary, positive real roots are found only if $A^2 > C^2$. Instability occurs only if this condition is satisfied, and the growth rate is then $\Gamma/2\pi l^2(A^2 - C^2)^{1/2}$. Other disturbances are neutral. Substituting $\phi = \pi X$ and $2\pi k = Y$ it may easily be shown that the condition for instability is

$$\left(\cosh Y - \frac{X^2 \sinh Y}{2}\right)^2 > (\cosh XY \cosh Y - X \sinh XY \sinh Y)^2 \quad (4)$$

in $0 < Y < \infty$ and $0 \leqslant X \leqslant 1$, this is satisfied for all X if

$$Y > \cosh^{-1} 3. \quad (5)$$

Figure 4 shows the stability curve, derived numerically from Eq. (4), and the nondimensional growth rates $(A^2 - C^2)^{1/2}$. The vortex separation, l, corresponds to the Langmuir cell width so that the separation of surface convergence zones (or windrows) is $2l$. If the depth of the center of the vortices, h, is less than $0.281l$, the vortex will be stable to all two-dimensional disturbances. The most unstable mode, that having the largest growth rate for fixed $Y = 2\pi h/l$, is the one with $X = 1$ ($\phi = \pi$). This is also the first mode of instability to become unstable as Y increases to a value greater than $\cosh^{-1} 3$ and corresponds to a disturbance with wavelength $2l$, similar to the "pairing" mode of instability observed to dominate in the growth of a free shear layer represented by a line of parallel vortices all of the same sign.

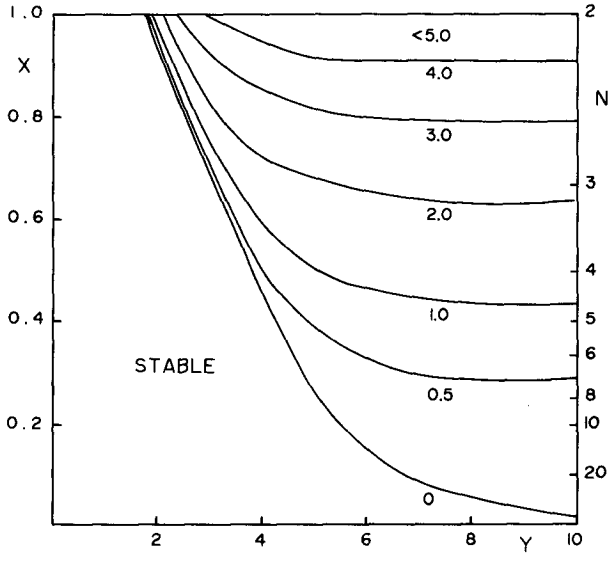

FIG. 4. The stability curve and growth rates for two-dimensional disturbances to a vortex array at distance h from a plane boundary. The horizontal coordinate is $Y = 2\pi h/l$ where l is the separation of the vortices, and the vertical coordinate is $X = \phi/\pi$ where $\phi = 2\pi l/$ (wavelength of the disturbance). The number, N, of vortices per wavelength is shown at the right. The dimensional growth rates are found by multiplying the values shown by $\Gamma/2\pi l^2$.

A three-dimensional perturbation involves both the displacements in x_n and z_n described above and a further y displacement, y_n, of a vortex element. The corresponding displacements of the image vortices are $(x_n, y_n, -z_n)$. The major source of complexity is that, as described by Crow (1970) and RS, a vortex will now suffer from a self-induced interaction that produces singularities. These can be avoided by supposing that it has a finite core of radius a. Following RS we suppose that within the core the vorticity is uniform (in their notation, $f = 1$) and that the core radius is small compared to the separation length l.

We derive three equations describing the motion of a selected vortex element in the three directions x, y, and z, which are linearized as before. We can now specify disturbances to the position coordinates x_n, y_n, z_n, which are proportional to α, β, and γ times $\exp(in\phi + im\rho_n$, respectively, where ρ_n is a Lagrangian variable, $-\infty < \rho_n < \infty$, and m is an axial wavenumber. The y equation decouples from the x and z equations, which can then be written as expressions relating α and β,

$$\frac{2\pi l^2}{\Gamma}\frac{d\alpha}{dt} = -(A - C - \eta)\beta - B\alpha, \quad (6)$$

$$\frac{2\pi l^2}{\Gamma}\frac{d\beta}{dt} = -(\tilde{A} + \tilde{C} + \eta)\alpha - B\beta, \quad (7)$$

where

$$A = -\frac{\pi^2}{6} + \frac{\pi^2 \cosh\kappa\pi}{\sinh^2\kappa\pi} - 2\sum_{q=1}^{\infty}(-1)^q \frac{\psi(qs)\cos q\phi}{q^2},$$

$$B = 2i\sum_{q=1}^{\infty}(-1)^q \frac{\kappa[\chi(\tau) + \psi(\tau)]}{(q^2 + \kappa^2)^2}\sin q\phi,$$

$$C = -\frac{\chi(\kappa ml)}{\kappa^2} + 2\sum_{q=1}^{\infty}(-1)^q \frac{[q^2\psi(\tau) - \kappa^2\chi(\tau)]}{(q^2 + \kappa^2)^2}\cos q\phi,$$

$$\chi(x) = xK_1(x), \quad \psi(x) = x^2K_0(x) + xK_1(x),$$

$$\kappa = 2h/l, \quad \tau = (q^2 + \kappa^2)^{1/2}ml,$$

and where K_0, K_1 are the modified Bessel functions of the second kind,

$$\eta = \frac{(ml)^2}{2}\left[\ln\frac{2}{ma} - \gamma_1 + \frac{1}{4}\right],$$

where $\gamma_1 = 0.5772$ is Euler's constant. The quantities with tildes can be found by interchanging χ and ψ in the expressions for A and C. [These equations are derived with a little algebra from (2.9) to (2.15) given by

RS.] These equations reduce to the set of equations (2) and (3) found above if ml tends to zero, that is, if the wavelength of the axial disturbance, $2\pi/m$, tends to infinity.

Seeking again an exponential solution α and $\beta \propto \exp pt$ we find $p = (\Gamma/2\pi l^2)\{-B \pm [(A - C - \eta)(\tilde{A} + \tilde{C} + \eta)]^{1/2}$ so that, since B is pure imaginary, we have growing solutions provided that $V \equiv (A - C - \eta)(\tilde{A} + \tilde{C} + \eta) > 0$. The growth rate nondimensionalized with $\Gamma/2\pi l^2$ is $V^{1/2}$.

We have determined numerically the stability boundaries $V = 0$ and nondimensional growth rate at $ml = 0.5$ and $ml = 1.0$ taking $ma = 0.1$, and these are shown in Fig. 5. Comparison with Fig. 4, which corresponds to $ml = 0$, shows that the introduction of a degree of freedom in which the vortices can wave or meander along their length allows an instability to develop in the previously stable zone at small values of h/l. These have maximum growth rates at zero values of ϕ and correspond to a collective instability in which the vortices all meander together. At very small values of Y there remains a zone of stability. Another effect of allowing alongaxis waves is to stabilize the unstable region at large Y and small ϕ, raising the stability boundary from its near zero ϕ position in Fig. 4 to a value of $\phi = 0.45\pi$ at $ml = 1.0$ in Fig. 5b.

We have examined the maximum growth rate at $\phi = \pi$ as a function of ml. At $Y = 5$ the maximum growth rate lies between $ml = 0$ and $ml = 0.1$. However, as Y decreases the maximum growth rate is found at increasing values of ml, reaching $ml = 0.5$ at $Y = 1.9$ and $ml = 1$ at $Y = 1.82$. The mode with the maximum growth rate in the pairing mode has an axial wavelength that is very much greater than the vortex separation if the vortices are deep (h/l large), but that decreases as the vortices come closer to the surface.

The effect of varying a/l appears to be small. For example, at $X = 0.3$ ($\phi = 0.3\pi$), the stability boundary at $ml = 0.5$ varies for $Y = 3.9$ to 4.2 as a/l varies from 0.05 to 0.2.

b. A vortex array in a layer of finite depth

In practice the field of motion associated with Langmuir circulation is of limited vertical extent, extending at most to the sea or lake bed or to the thermocline in stratified waters. Therefore, it is appropriate to consider the stability of a vortex array confined between horizontal boundaries. For simplicity we suppose that both are stress free and rigid, separated by a distance h (the thermocline or lake depth), and that the vortices are located at middepth. The case considered in section 2a may be regarded as an appropriate limit in the early stages of circulation, when mixing has not yet extended to the depth of a preexisting homogeneous layer, or in which the depth of the center of the circulation pattern is much less than the depth, while the present case applies to the mature, fully evolved circulation pattern, which is thoroughly mixed to full depth or to the thermocline.

If we now take the position of the vortices in the array to be $x = nl$, $z = 0$ with $n = 0, \pm1, \pm2, \cdots$ and the vortex strength to be $(-1)^n\Omega$, then the image array required to satisfy the boundary conditions of no normal flow through the boundaries at $z = \pm h/2$ is the infinite array with vortices of strength $(-1)^{n+j}\Omega$ located at $x = nl$, $z = jh$; $j = \pm1, \pm2, \cdots$ (Fig. 6).

The stability of this array to two-dimensional perturbations has been considered by Rosenhead (1929;

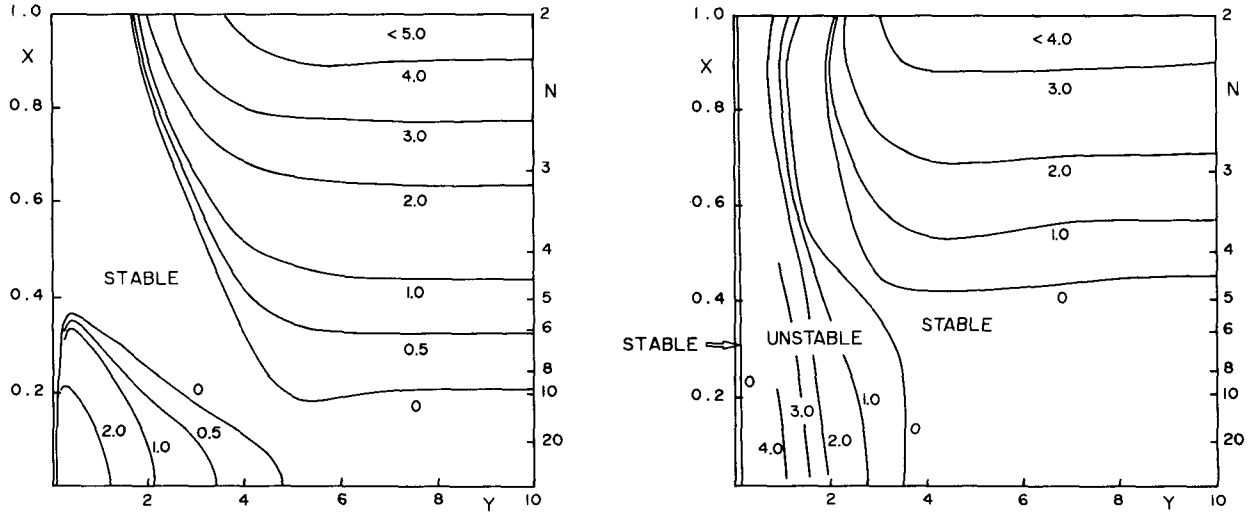

FIG. 5. Stability curves and growth rates for three-dimensional disturbances to a vortex array at distance h from a plane boundary. (a) and (b) show $ml = 0.5$ and 1.0, respectively, where m is the wavenumber of the alongaxis disturbance and l is the vortex separation. The parameter $a/l = 0.1$. The coordinates are as in Fig. 4.

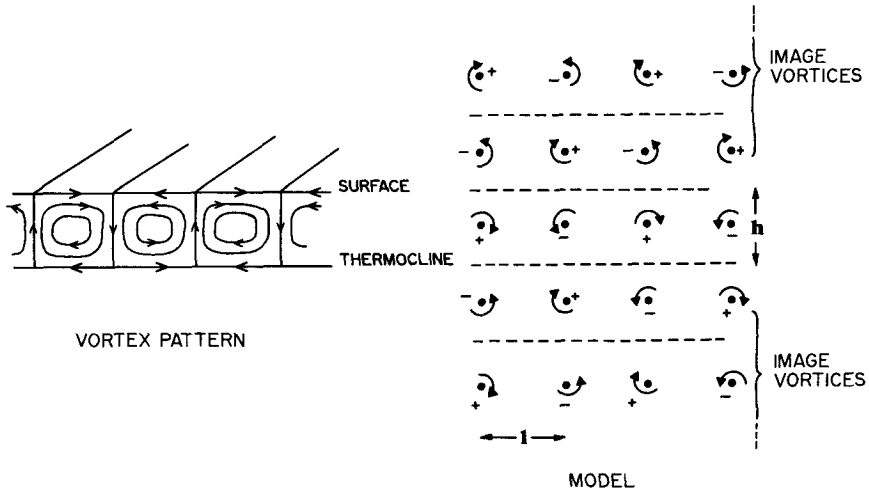

FIG. 6. Sketch of the vortex pattern and model image field for a set of parallel vortices midway between plane boundaries separated by a distance h.

he also examined more complex distributions of vortices). Stability is found if $h/l < 0.709$, or if the depth of the center of the vortices, $h/2$, is less than $0.354l$. This is greater than the value found as the stability limit in section 2a; an effect of the lower boundary is to extend the range of stability; that is, to stabilize a range of vortex depth to vortex separation ratios that was previously unstable.

The stability characteristics can be calculated using the procedure described in section 2a. This leads to equations similar to Eqs. (2) and (3) but in which the terms, A, B, and C are now infinite series in j, the z position coordinate. The condition for instability is again given by $A^2 > C^2$ where now

$$A = \sum_{q=1}^{\infty} \frac{\cosh 2qYX \cosh 2qY}{\sinh^2 2qY} - \frac{X^2}{4} - \sum_{q=1}^{\infty} (-1)^q \frac{\cosh qY}{\sinh^2 qY} - X \sum_{q=1}^{\infty} \frac{\sinh 2qXY}{\sinh 2qY},$$

$$C = X \sum_{q=0}^{\infty} \frac{\sinh(2q+1)XY}{\sinh(2q+1)Y} - \sum_{q=0}^{\infty} \frac{\cosh(2q+1)XY \cosh(2q+1)Y}{\sinh^2(2q+1)Y}$$

and where $Y = \pi h/l$ and $0 \leq X = \phi/\pi \leq 1$ as before.

The stability curve and growth rates are shown in Fig. 7. The most unstable mode, that having the largest growth rate, is again the pairing mode with a wavelength $2l$. Comparison with Fig. 4 shows that the growth rates are less than those found in the unbounded fluid at similar values of h/l; the effect of the lower boundary is to reduce growth rates or stabilize the instability.

A three-dimensional perturbation may also be analyzed in a manner similar to section 2a with a resulting pair of equations identical to (6) and (7) but with

$$A = -\frac{\pi^2}{6} - 2 \sum_{q=1}^{\infty} (-1)^q \frac{\psi(qml)}{q^2} \cos q\phi - 2 \sum_{q=1}^{\infty} (-1)^q \frac{\pi^2 \cosh q\kappa\pi}{\sinh^2 q\kappa\pi}$$

and

$$C = 4 \sum_{n=1}^{\infty} \sum_{q=1}^{\infty} (-1)^q \frac{[q^2\psi(\tau) - n^2\kappa^2 X(r)]}{(q^2 + n^2\kappa^2)^2} \cos q\phi - 2 \sum_{q=1}^{\infty} \frac{X(q\kappa ml)}{q^2\kappa^2};$$

$\tilde{A}$ is found by writing χ for ψ in the expression for A, and $\tilde{C}$ is given by

$$\tilde{C} = 2 \sum_{q=1}^{\infty} (-1)^q \frac{\psi(q\kappa ml)}{q^2\kappa^2} - 4 \sum_{n=1}^{\infty} (-1)^n \times \left\{ \sum_{q=1}^{\infty} (-1)^q \frac{[q^2 X(r) - n^2\kappa^2\psi(r)]}{(q^2 + n^2\kappa^2)^2} \cos q\phi \right\},$$

where m is again the axial wavenumber and $\kappa = h/l$. As before, there is a growing disturbance with nondimensional growth rate $V^{1/2}$ if

$$V \equiv (A - C - \eta)(\tilde{A} + \tilde{C} + \eta) > 0.$$

Convergence of the series is quite rapid except near $\phi = \pi$, and good numerical approximations may be computed using available NAG library routines with generally better than 1% accuracy. Figure 8 shows the stability curves and growth rates at $ml = 0.5$ and $ml = 1.0$, taking $a/l = 0.1$ as before. The general behavior is similar to that observed in the semi-infinite fluid

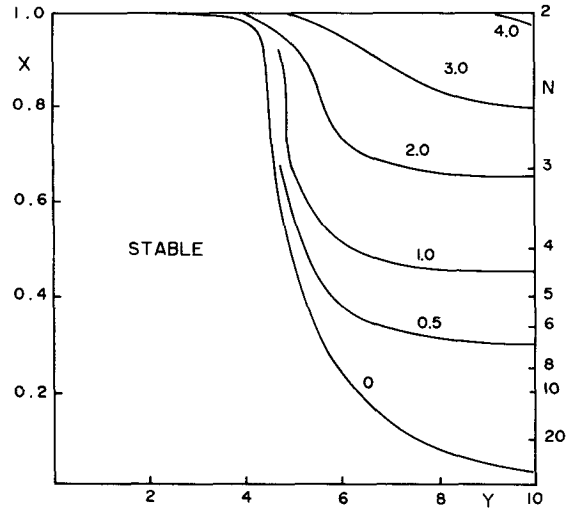

FIG. 7. The stability curve and growth rates for two-dimensional disturbances to a vortex array midway between parallel boundaries separated by distance h. The horizontal coordinate is $Y = \pi h/l$ where l is the distance between vortices, and the vertical coordinate $X = \phi/\pi$ (as before). The number of vortices per wavelength of the instability is N.

(Fig. 5), with the development of collective modes with large growth rates at the smaller values of $Y = \pi h/l$. At large Y the greatest growth rates are in the pairing mode, as before. Here, however, near $\phi = \pi$ (or $X = 1$ in the figures) and at $Y > 3$, larger growth rates occur at $ml = 0.5$ than at $ml = 0$ or at $ml = 1.0$; the fastest-growing modes occur at smaller axial wavelengths than in the semi-infinite fluid. This is confirmed by Fig. 9, which shows growth rates in the Y versus ml plane at $\phi = 0.9\pi$. (This value was chosen to avoid any uncertainty introduced by the slow convergence of series at $\phi = \pi$ and is sufficient for our purpose because we are trying here to provide only semiquantitative results. We are satisfied that the smooth approach of values to $\phi = \pi$ found in constructing Fig. 7 at $Y > 3$ indicates that there is no singular behavior at $\phi = \pi$ other than that involved in the slow convergent behavior of the expressions for C and $\tilde{C}$, and that the growth rates of $\phi = \pi$ are only slightly greater than at $\phi = 0.9\pi$.)

The maximum growth rate is found at increasing values of ml as Y decreases; for a fixed vortex separation, l, the axial wavelength of the fastest-growing disturbance decreases as the depth of the mixed layer decreases. The largest growth rates increase as the depth increases.

We have examined the sensitivity of these results to changes in the chosen value a/l, which represents the nondimensional size of the vortex core. As found in section 2a, the stability boundary is little changed, varying from $Y = 4.7$ to 4.95 as a/l varies from 0.05 to 0.2 at $\phi = 0.3\pi$, and by a lesser amount at greater ϕ. The maximum growth rates at $\phi = 0.9\pi$, $3 < Y < 10$, vary by less than 1% for a doubling in a/l. The largest variation in growth rates were found at $Y = 1$ and $ml = 1$, being an increase of about 4% for a change in a/l from 0.1 to 0.2. Therefore, it appears that the results are insensitive to the selection of the size of the vortex core provided that it is small compared to the disturbance wavelength.

3. Discussion

The objective of the analysis described above is to obtain insight into the way in which the pattern of Langmuir circulation may become unstable. We have made some gross assumptions to enable us to adopt a simple approach while retaining some essential features

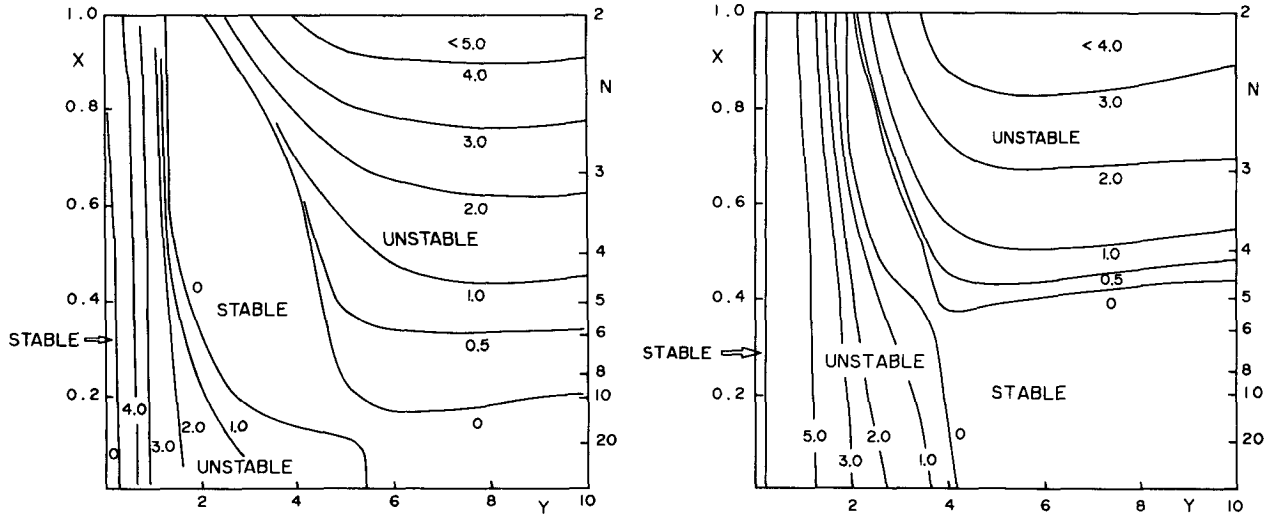

FIG. 8. Stability curves and growth rates for three-dimensional disturbances to a vortex array midway between parallel boundaries. The axes are as in Fig. 7. (a) and (b) show curves at $ml = 0.5$ and 1.0, respectively. The parameter $a/l = 0.1$.

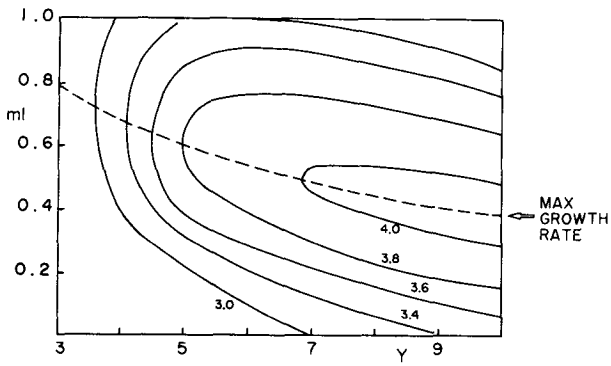

FIG. 9. The growth rates as functions of $Y = \pi h/l$ and nondimensional axial wavenumber, ml, for vortices separated by distance l lying at middepth between horizontal planes a distance h apart and at $\phi = 0.9\ \pi$. The dashed curve shows the maximum growth rate. The parameter $a/l = 0.1$.

of the flow. Not least among the assumptions are that the vortices are of equal strength, are equally spaced, are infinite in number and in downwind extent, and that the forcing that determined their generation is diminished or no longer dominant in determining their mutual interactions. We ignore such effects as cross-wind drift (section 1), tilted internal structure (Thorpe and Hall 1982) or other asymmetrical flow structure within cells, and small-scale turbulence.

A wide range of values of the ratio of windrow spacing, $L = 2l$, to thermocline depth (or, for shallow lakes, total depth), h, has been observed. Faller and Caponi (1978) review oceanic values, which range from about 0.3 to 2, while Leibovich (1983) reports values that range between 0.66 and 1.66. Smith et al. (1987) found convergence zones with a separation ratio of about 3. It appears that the size distribution of the circulation pattern is generally multimodal, with a variety of superimposed scales as observed in Fig. 1. The higher values of the ratio probably represent the "dominant" scales that occur once the structure has developed, and when a pattern like that sketched in Fig. 6 is produced. (The smaller scales may be more appropriately represented by the pattern sketched in Fig. 3.) The range of values given by Leibovich corresponds to values of Y in Figs. 7–9 of 9.5 to 3.8, respectively. (Faller and Caponi's range is broader, from 21 to 3.1.) This range of Y is one in which the growth rates are generally moderate, between the large values of the collective mode at small Y and the increasingly large values at large Y. Perhaps this contributes a reason for the existence of the circulation pattern's limited range of scales. In this range the theory outlined above shows, however, that the circulation pattern should be unstable, with a fastest-growing mode that corresponds to a pairing of vortices with alongaxis wavelength to windrow separation, π/ml of (taking Leibovich's range, for example) 8.1 to 4.6, respectively, in reasonable agreement with estimates. The corresponding nondimensional growth rates are about 4 to 3, respectively. These correspond to dimensional values of e-folding growth times of $\pi L^2/2\Gamma$ divided by 4 or 3, respectively, where Γ is the strength of the equivalent vortex.

We may estimate Γ by noting that the surface current, u, immediately above a vortex core can be found by summing over the array of vortices shown in Fig. 6. It may be shown (using summations given by Bromwich 1955) that

$$u = \frac{2\Gamma}{L} \sum_{q=0}^{\infty} \frac{(-1)^q}{\sinh(q + 1/2)Y},$$

which can be determined approximately as $0.6\Gamma/L$ at $Y = 3.8$ or $0.03\Gamma/L$ at $Y = 9.5$, and hence, we can determine the growth times in terms of u as $0.314L/u$ and $0.013L/u$ at $Y = 3.8$ and 9.5 or $L/h = 1.66$ and 0.66, respectively. We conclude, therefore, that given a separation of windrows of 20 m and convergence speeds of 5 cm s^{-1} (Fig. 1), the typical time scales for instability (say 10 times the e-folding time scale) lie between 0.9 and 21 min. The upper end of this band corresponding to larger values of L/h seems consistent with observations described in section 1; the lower end, corresponding to small values of L/h, appears to be unrealistically small, perhaps implying that cells of such dimensions can, at best, be transient. A more appropriate measure of the unstable nature of the vortex pattern associated with Langmuir circulation is that provided by the periods of time (2–30 min; Leibovich 1983) that are taken for a set of windrows to disappear and for a new set to become reestablished and reorientated following a sudden change in wind direction. The observed time response for cells of different scales has been reviewed by Faller and Auer (1988; see their Fig. 3), and is about 11 min for 20-m scales. This period is consistent with those predicted here for vortices to become unstable if left, without forcing, to interact with each other.

A description of the finite-amplitude evolution of the instability and the breakup of the Langmuir cells is beyond the scope of the linear, inviscid, small-amplitude theory, but we may conjecture on what occurs. In the "pairing" instability of a vortex sheet, vortices (all of the same sign) amalgamate in pairs, enhancing the vorticity at each new center and doubling the distance between vortex centers. Here, however, the pairing vortices are of opposite signs and pairing, together with turbulent dissipation, may result in a cancellation of vorticity. If the pairing, or amalgamation, occurs between two vortices lying between windrows, the net circulation in that region will be suppressed and one might expect a diffusive growth of the neighboring cells to occur to fill the intermediate region, resulting in an apparent amalgamation of windrows (Fig. 10a). If, however, the pairing vortices lie on either side of a windrow, their amalgamation and the cancellation of circulation will remove the convergent flow supporting the windrow and subsurface bubble band, which will therefore terminate without amalgamation with a

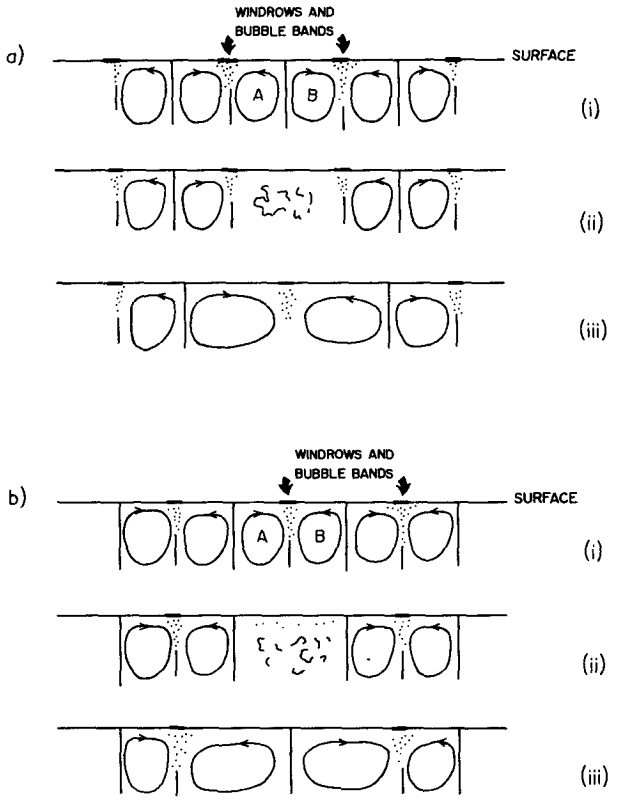

FIG. 10. (a) Amalgamation of bubble bands by vortex pairing. "Cells" or vortices at *A*, *B* in (i) combine as sketched in (ii) with a weakening and cancellation of the circulation and dissipation of energy by turbulence. Adjoining cells spread diffusively, carrying the associated windrows and bubble bands to join together at (iii). (b) Termination of bubble bands by vortex pairing. The vortex pair *A*, *B* in (i) amalgamate as sketched in (ii), with the removal of surface convergence and downwelling leading to the dispersal of bubbles and the disappearance or termination of the bubble band. Adjoining cells may spread diffusively as in (iii), but their sense of circulation is not such as to reestablish the windrow.

neighboring band (Fig. 10b). Both processes are seen in Fig. 2. Even in the relatively well controlled environment of the laboratory, the amalgamation of vortices by pairing in Kelvin–Helmholtz instability does not occur everywhere simultaneously (see, for example, Thorpe 1971, Fig. 5), so that the disappearance of bubble bands or their amalgamation may occur in a rather random way, as is observed. There appears to be an equal likelihood of the pairing of windrows that lie on either side of a surface convergence or of a divergence zone, so the termination of bubble bands should occur about as frequently as does the amalgamation of bands, as is seen in Fig. 2.

We conclude the following:

(i) There are two favored modes of instability of uniform vortex arrays taken to represent Langmuir circulation. The first is found when the vortex separation, L, is large in comparison with the depth of the vortex core or the water, or thermocline, depth, h. Vortices then oscillate together collectively with a nonzero alongaxis wavenumber and large growth rates (Figs. 5 and 8). In the second mode at larger values of h/L, vortices are involved in "pairing." Here the fastest-growing mode has an axial wavelength that decreases as h/L decreases.

(ii) Growth rates are reduced at equivalent values of h/L, in the presence of a thermocline, with stable modes occurring when motion is two-dimensional (zero axial wavenumber) provided h/L is sufficiently small.

(iii) Within the reported range of values, and for a mixing layer bounded by a thermocline, the fastest-growing waves are predicted to correspond to a pairing mode, and pairing is indeed observed (Fig. 2). The downwind scale is predicted to be 4.6 to 8.1 times the windrow separation, with the values increasing as the windrow spacing decreases in comparison with the thermocline depth. This prediction is of the right order of magnitude, but more observations are needed. The growth rates are predicted to increase linearly as the circulation increases at fixed scales of L and h, and have values that appear to be somewhat larger than observations suggest under conditions of steady forcing, but that are quite consistent with the time taken for structure to be lost when changes in wind direction occur.

The simple theory, however, provides at best an order-of-magnitude estimate of the growth rates, and a qualitative description of the structure of the unstable modes, because of the radical assumptions that have been made to produce this simplistic model. Further work is essential if the processes causing pairing and other pattern variations leading to dispersion in Langmuir circulation are to be adequately described, quantified, and understood.

Acknowledgments. Figures 1 and 2 were kindly provided by Mr. Marcel Curé in the Department of Oceanography, Southampton University. A full report of this work is in preparation. It was carried out with support from the US Office of Naval Research under Contract N00014-90-J-147 and from the UK National Environment Research Council.

REFERENCES

Bromwich, T. J. I'A., 1955: *An Introduction to the Theory of Infinite Series.* Macmillan, 356–364.

Crow, S. C., 1970: Stability theory for a pair of trailing vortices. *A.I.A.A.J.*, **8,** 2172–2179.

Csanady, G. T., 1974: Turbulent diffusion and beach deposition of floating pollutants. *Advances in Geophysics,* Vol. 18A, Academic Press, 371–381.

Faller, A. J., and E. A. Caponi, 1978: Laboratory studies of wind-driven Langmuir circulations. *J. Geophys. Res.*, **83,** 3617–3633.

——, and S. J. Auer, 1987: The roles of Langmuir circulation in the dispersion of surface tracers. *J. Phys. Oceanogr.*, **18,** 1108–1123.

Lamb, H., 1932: *Hydrodynamics.* Cambridge University Press.

Langmuir, I., 1938: Surface motion of water induced by wind. *Science,* **87,** 119–123.

Leibovich, S., 1983: The flow and dynamics of Langmuir circulations. *Ann. Rev. Fluid Mech.*, **15,** 391–427.

——, and S. Paulucci, 1980: The Langmuir circulation instability as a mixing mechanism in the upper ocean. *J. Phys. Oceanogr.*, **10,** 186–207.

——, S. K. Lele, and I. M. Moroz, 1989: Non-linear dynamics in Langmuir circulations and in thermosolutal convection. *J. Fluid Mech.*, **198,** 471–511.

Moroz, I. M., and S. Liebovich, 1985: Oscillatory and competing instabilities in a non-linear model for Langmuir circulations. *Phys. Fluids,* **28,** 2050–2061.

Pollard, R. T., 1977: Observations and theories of Langmuir circulations and their role in near surface mixing. *A Voyage of Discovery: G. Deacon 70th Anniversary Volume,* M. Angel, Ed., Pergamon, 235–251.

Robinson, A. C., and P. G. Saffmann, 1982: Three-dimensional stability of vortex arrays. *J. Fluid Mech.*, **125,** 411–427.

Rosenhead, L., 1929: The Karman street of vortices in a channel of finite breadth. *Phil. Trans. Roy. Soc. London,* **228,** 275–330.

——, 1930: The spread of vorticity in the wake behind a cylinder. *Proc. Roy. Soc. London, Ser A,* **127,** 590–612.

Smith, J., R. Pinkel, and R. Weller, 1987: Velocity structure in the mixed layer during MILDEX. *J. Phys. Oceanogr.*, **17,** 425–439.

Thorpe, S. A., 1971: Experiments on the instability of stratified shear flows: Miscible fluids. *J. Fluid Mech.*, **46,** 299–319.

——, 1984: The effect of Langmuir circulation on the distribution of submerged bubbles caused by breaking wind waves. *J. Fluid Mech.*, **142,** 151–170.

——, and A. J. Hall, 1982: Observations of the thermal structure of Langmuir circulation. *J. Fluid Mech.*, **114,** 237–250.

——, and ——, 1983: The characteristics of breaking waves, bubble clouds and near-surface currents observed using side-scan sonar. *Contin. Shelf Res.*, **1,** 353–384.

——, ——, A. R. Packwood, and A. R. Stubbs, 1985: The use of a towed side-scan sonar to investigate processes near the sea surface. *Contin. Shelf Res.*, **4,** 597–607.

von Kármán, T., 1911: Uber den Mechanisms des Widerstands, den ein bewegter Korper in einer Flussigkeit erfahrt. Gottenger Nachrichten, *Math. Phys.*, **k1,** 509–517.

——, 1912: Uber den Mechanisms des Widerstands, den ein bewegter korper in einer Flussigkeit erfahrt. Gottenger Nachrichten, *Math. Phys.*, **k1,** 547–556.

Weller, R. A., and J. F. Price, 1988: Langmuir circulation within the oceanic mixed layer. *Deep-Sea Res.*, **35,** 711–747.